Solar Phys (2008) 248: 233–245
DOI 10.1007/s11207-007-9056-9

Widespread Occurrence of Trenching Patterns in the Granulation Field: Evidence for Roll Convection?

A.V. Getling · A.A. Buchnev

Received: 29 April 2007 / Accepted: 20 September 2007 / Published online: 26 October 2007

Abstract Time-averaged series of granulation images are analysed using COLIBRI, a purpose-adapted version of a code originally developed to detect straight or curvilinear features in aerospace images. The image-processing algorithm utilises a nonparametric statistical criterion that identifies a straight-line segment as a linear feature (lineament) if the photospheric brightness at a certain distance from this line on both sides is stochastically lower or higher than at the line itself. Curvilinear features can be detected as chains of lineaments, using a modified criterion. Once the input parameters used by the algorithm are properly adjusted, the algorithm highlights "ridges" and "trenches" in the relief of the brightness field, drawing white and dark lanes. The most remarkable property of the trenching patterns is a nearly universally present parallelism of ridges and trenches. Since the material upflows are brighter than the downflows, the alternating, parallel light and dark lanes should reflect the presence of roll convection in the subphotospheric layers. If the numerous images processed by us are representative, the patterns revealed suggest a widespread occurrence of roll convection in the outer solar convection zone. In particular, the roll systems could form the fine structure of larger scale, supergranular and/or mesogranular convection flows. Granules appear to be overheated blobs of material that could develop into convection rolls owing to instabilities of roll motion.

Keywords Sun: photosphere · Sun: granulation

1. Introduction

Getling and Brandt (2002) reported that images of solar granulation averaged over time intervals as long as, *e.g.,* two hours, are far from completely smeared but contain bright,

A.V. Getling (✉)
Institute of Nuclear Physics, Lomonosov Moscow State University, 119991 Moscow, Russia
e-mail: a.getling@mail.ru

A.A. Buchnev
Institute of Computational Mathematics and Mathematical Geophysics, 630090 Novosibirsk, Russia
e-mail: baa@ooi.sscc.ru

granular-sized blotches, which may form quasiregular systems of concentric rings or parallel strips – "ridges" and "trenches" in the brightness field – on a meso- or supergranular scale. Getling (2006) implemented a detailed investigation of such long-lived patterns and found that they do not appear unusual in images averaged over one- to two-hour time intervals.

These systems resemble some specific types of the roll patterns known from laboratory experiments on Rayleigh – Bénard convection and may reflect the fine structure of subphotospheric convection cells. If the time variations of intensity are traced at the point corresponding to a local intensity maximum in the averaged image (near the centre of a light blotch) and at a nearby local-minimum point, a remarkable pattern of correlations between these variations can be noted. In some cases, the correlations are periodic functions of the time lag or a tendency to anticorrelation is observed. This fact supports our suggestion (Getling, 2000) that granules are hot blobs of the solar plasma carried by the convective circulation and that they can even reemerge on the photospheric surface.

Since the quasiregular structures manifest themselves in time-averaged images, they should be associated with a long-lived component of the granulation field. Getling and Brandt (2002) and Brandt and Getling (2004) noted that the decrease in the rms contrast of the averaged images with the averaging time $[t]$ is considerably slower compared to the statistical $t^{-1/2}$ law, and this fact was regarded as a particular argument for the presence of long-lived features.

In his comment on the original paper by Getling and Brandt (2002), Rast (2002) suggested that the structures in the granulation field are merely of a statistical nature and do not reflect the structure of real flows. He constructed a series of artificial random fields with some characteristic parameters typical of solar granulation and found some similarities between the properties of these fields and of the real granulation patterns. On this basis, Rast raised doubts about the existence of the long-lived component in the granulation dynamics. A detailed discussion of Rast's criticism given by Getling (2006) invokes, in particular, the contrast-variation analysis (Brandt and Getling, 2004). A number of counterarguments are presented and it is shown that Rast's considerations cannot be applied to the real granulation patterns.

As noted by Getling and Brandt (2002), signatures of the prolonged persistence of some features in the granulation patterns have already been observed previously. Roudier *et al.* (1997) detected long-lived singularities – "intergranular holes" (dark features) – in the network of supergranular lanes. Such holes were continuously observed for more than 45 minutes, and their diameters varied from $0.24''$ (180 km) to $0.45''$ (330 km). Hoekzema, Brandt, and Rutten (1998) and Hoekzema and Brandt (2000) also studied similar features, which could be observed for 2.5 hours in some cases. Baudin, Molowny-Horas, and Koutchmy (1997) attributed the blotchy appearance of a 109-minute-averaged granulation image to a sort of persistence of the granulation pattern; alternatively, this effect can be interpreted in terms of the recurrent emergence of granules at the same sites (Getling, 2006).

Some indications of a long-term spatial organisation in the granulation field have also been revealed in observations. Dialetis *et al.* (1988) found that granules with longer lifetimes exhibit a tendency to form mesogranular-scaled clusters. Muller, Roudier, and Vigneau (1990) also detected such clustering in the spatial arrangement of large granules; they emphasised a plausible relationship between the clusters and mesogranules. Roudier *et al.* (2003) reported their observations of a specific collective behaviour of families ("trees") of fragmenting granules. Such families can persist for up to eight hours and appear to be related to mesogranular flows. An imprint of the supergranulation structure can also be traced in the granulation pattern (Baudin, Molowny-Horas, and Koutchmy, 1997).

Based on their analysis of pair correlations in the supergranular and granular fields, Berrilli *et al.* (2004) reported a finding that bears some similarity with ours. Specifically,

the probability of finding a target supergranule or granule (identified by its barycentre) at a given distance from the barycentre of a chosen reference supergranule or granule is an oscillating function of this distance with a local amplitude decreasing from some maximum (reached at a small distance). This reflects a specific kind of order in the supergranulation and granulation patterns, which is consistent with the presence of concentric-ring structures.

It is remarkable that an effect of spatial ordering has also been detected on a supergranular scale. Lisle, Rast, and Toomre (2004) revealed a persistent alignment of supergranules in a meridional direction reminiscent of the alignment of light blotches described by us. There is also a parallelism in the interpretation of the quasiregularity in the granulation and supergranulation fields: Whereas we are inclined to interpret the trenching patterns as the manifestation of a fine structure of the supergranular flows, Lisle, Rast, and Toomre (2004) attribute the alignment of supergranules to an ordering influence of giant convection cells.

Here, we employ a specific image-processing algorithm to analyse granulation patterns and investigate their spatial organisation. In particular, the results of our study show that the arrangement of granules may assume various forms, and the patterns of light blotches detectable in the averaged images have a common feature – a nearly universally present parallelism of alternating light and dark lanes. If the images analysed by us are representative, the trenching patterns could naturally be interpreted as manifestations of roll convection entraining granules; this form of motion proves to be widespread in the upper subphotospheric layers.

2. The Data

We mainly deal with excellent images of the photosphere from the well-known La Palma series obtained by Brandt, Scharmer, and Simon (see Simon *et al.*, 1994) on 5 June 1993 using the Swedish Vacuum Solar Telescope (La Palma, Canary Islands). Specifically, we use a seven-hour subset of this series and a 43.5×43.5 Mm^2 subfield (480×480 pixels of size 90.6 km) of the original images. The observed area was located not far from the disk centre, and the images were produced by the telescope in the 10-nm-wide spectral band centred at a wavelength of 468 nm. The resolution was typically no worse than about $0.5''$, and the frame cadence was 21.03 seconds.

Previously (Getling and Brandt, 2002; Getling, 2006), we already described the principal elements of the data acquisition and preprocessing techniques employed by Simon *et al.* (1994). Here, we only briefly recall that the images were aligned, destretched, and cleaned from rapid intensity variations by means of subsonic filtering. Furthermore, all of them were normalised to the same value of the rms contrast, and the residual large-scale intensity gradients were removed from them.

We give here our primary attention to granulation fields averaged over one- to two-hour intervals.

In addition to the data of the La Palma series, we use here an averaged image from the subsonically filtered version of the 45.5-hour series obtained using the SOHO MDI instrument in 1997, from 17 January 00:01 UT to 18 January 21:30 UT (see Shine, Simon, and Hurlburt, 2000). This series contains white-light images with a resolution of about $1.2''$ taken at a one-minute interval. We present here an enlarged 87×70 Mm^2 cutout (200×160 pixels) of the selected image.

3. Image Processing

In our analysis, we use the COntours and LIneaments in the BRIghtness field (COLIBRI) code, a purpose-adapted version of a code constructed previously at the Institute of Computational Mathematics and Mathematical Geophysics (Novosibirsk, Russia) and intended for the detection of linear and circular structures in aerospace images (a design that has been successfully employed for several years). The code is an implementation of certain statistical criteria for the detection of stretched features (in our case, linear structures and contour elements) against a random background. The underlying algorithm was developed by Salov (1997).

The principal reason for using such techniques is as follows. The random component of the processes under study clutters the observational data (*i.e.*, images) with random variations, which mask the brightness differences between the points of the object sought and of the background areas. Accordingly, reliable criteria for detection of objects should be based on a probabilistic (statistical) approach. The presence of an object in the image manifests itself in the fact that the random observable quantities in the object are *stochastically* – or, more simply, *systematically* – larger (or smaller) than in the background areas. The so-called nonparametric criteria, based on stochastic comparisons of the observables inside and outside the hypothetical object, do not depend on the (unknown) distributions of the observables and prove to be efficient for our purposes.

The COLIBRI code has two operation modes that enable the detection of either lineaments or contours in photospheric images.

A lineament (linear element) is a stretched, nearly linear object, blurred and nonuniform in brightness along its extent. To detect a lineament, the algorithm analyses (almost) all of its possible positions. For any trial position, to decide whether or not a lineament is present, the set of brightness values taken at some points along the hypothetical lineament of length l is compared with the two sets taken at the points located at a certain distance Δ on both sides of the lineament, at the normals intersecting it at the originally chosen points. Specifically, the algorithm checks the hypotheses that either all the sets of measured quantities are stochastically equal (no object is present) or, alternatively, the set of the central brightness values is stochastically greater (smaller) than the sets taken on both sides (an object is present). The nonparametric criterion used to test these hypotheses (Salov, 1997) is based on computing the values of the Mann – Whitney statistics (Mann and Whitney, 1947; Whitney, 1951).

A somewhat different approach is used in the detection of contours, by which are meant curvilinear features with *a priori* unknown shapes. In this case, the algorithm constructs the contours as chains of lineaments, but the criterion for their detection has a different form. Again, sets of brightness values are taken at normals to the trial lineament at a certain distance Δ on both sides of it. To decide whether or not an object is present, the algorithm checks the hypotheses that either the sets of brightness values taken on the two sides are stochastically equal (no object is present) or, alternatively, the values on one side are stochastically larger then the values on the other side (an object is present). In this case, the nonparametric criterion used to test these hypotheses is also based on the computed values of the Mann – Whitney statistics (Salov, 1997). In essence, a trial lineament is assumed to be a really present object provided the brightness gradient across it has some stochastically predominant sign. In this respect, the detected contours very crudely correspond to isohypses (horizontals) in a topographic contour map; however, they do not depend on the fine topographic details of the brightness field because the intensity values at a contour are not taken into account in constructing this contour.

The distance Δ, which is everywhere measured in pixels, is an input parameter of the algorithm. Other important parameters are the admissible probability of spurious detection of objects [p] and the range of admissible lengths of lineaments [l] (also expressed in pixels). The determination of the actual probability of spurious detection is fairly sophisticated (Salov, 1997), and describing it is beyond the scope of this paper.

Because of the noisy appearance of the analysed images, the detection procedure straightforwardly applied to an image may reveal a large number of spurious details. (By noise, we mean the presence of a multitude of light blotches interspaced by darker features, any of which, taken alone, is not representative from the standpoint of seeking quasiregular structures.) To reduce the noise level, a special filtering procedure was developed. It consists of two steps. First, any lineament is removed if it is completely covered by another one; at the same time, lineaments that partially overlap one another are combined into one lineament. Second, all lineaments that have no parallel neighbours (*i.e.,* do not belong to any bunch of lineaments) are also removed. The effect of filtering will be illustrated in the following (Figure 2).

4. Results

Our primary goal was to analyse structures in time-averaged series of granulation images. In addition, we attempted to process individual images, or snapshots. Signs of regularity can be visually noted in both cases; however, the snapshots contain many more fine details than do the averages, so that much more spurious features emerge when snapshots are processed. Here, we restrict ourselves to considering only the structures detected in averaged images.

The number of lineaments and contours detected in granulation images strongly depends on the chosen parameters of the image-processing procedure. It should be kept in mind that, generally, there is no combination of parameters that could be considered a universal optimum, applicable in any case. The optimum really depends on both the character of the analysed pattern and on the objective of analysis in any particular situation.

First, the optimum Δ value depends on the width of the linear features that are sought. Typically, we are seeking contours that correspond to parallel ridges and trenches in the relief of the brightness field. In the contour-detection mode, the COLIBRI code draws contours along the slopes and marks them as white or black curves depending on the direction of the slope (*i.e.,* on the stochastically predominant sign of the difference between the brightness values at the points located on the two sides of the contour at the same distance Δ). Usually, the code draws bunches of nearly parallel, closely located contours of either sort, which merge into white or black lanes. If Δ is small, the detected contours should gather near the steepest slope curve. However, as our experience shows (and as confirmed by some qualitative considerations), at larger Δ values comparable with some optimal, "resonant" distance related to the characteristic distance between ridges and trenches, the algorithm can output white lanes highlighting the ridges and dark lanes highlighting the trenches.

Similarly, there is no universally preferable value of the parameter p, which is regarded as the admissible probability of spurious detection. The optimum p is not universal and should be properly chosen for any processing regime specified by the other parameters.

The range of lineament lengths [l] used to construct contours has also some effect on the detection of structures. Generally, the algorithm can better integrate lineaments into contours for broader l ranges. However, the inclusion of very short lineaments results in a very high noise level. Moreover, the computation time grows dramatically with widening of the l range. Thus, a reasonable compromising choice should be made.

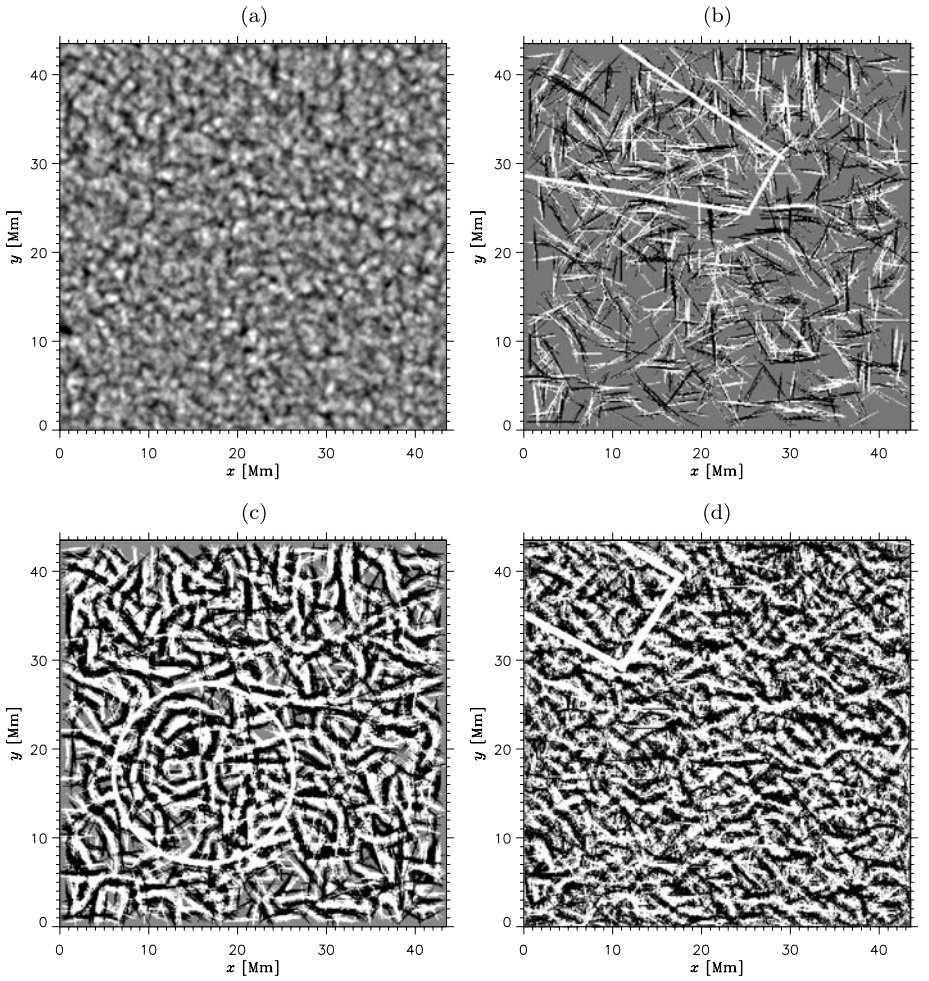

Figure 1 (a) A two-hour-averaged image and the results of contour detection in this image at (b) $p = 2.5 \times 10^{-4}$, $\Delta = 5$, $l = 16-43$; (c) $p = 2 \times 10^{-3}$, $\Delta = 8$, $l = 10-30$; and (d) $p = 10^{-2}$, $\Delta = 2$, $l = 5-20$.

Let us consider the two-hour-averaged image shown in Figure 1a and the structures detected in this image (Figures 1b – 1d). The last three panels are arranged in the order of increasing p; the largest Δ (= 8) is used in the case of panel c and the smallest Δ (= 2) in the case of panel d. As we can see, numerous patches of trenching patterns (not everywhere regular) with a characteristic width of ridges comparable to the granular size are clearly manifest in panel c. It is noteworthy that, in this figure, most white lanes are parallelled by one or more other white neighbouring lanes and at least two black neighbouring lanes. In other words, trenching patterns are very common in the image (although they vary widely in their area and in the number of alternating white and black lanes). A careful inspection of panel c shows that the black lanes really correspond to dark features in the images but not merely to background areas where no features have been detected (such areas are shown in grey). In panel d, the image processing everywhere highlights finer details of the pattern.

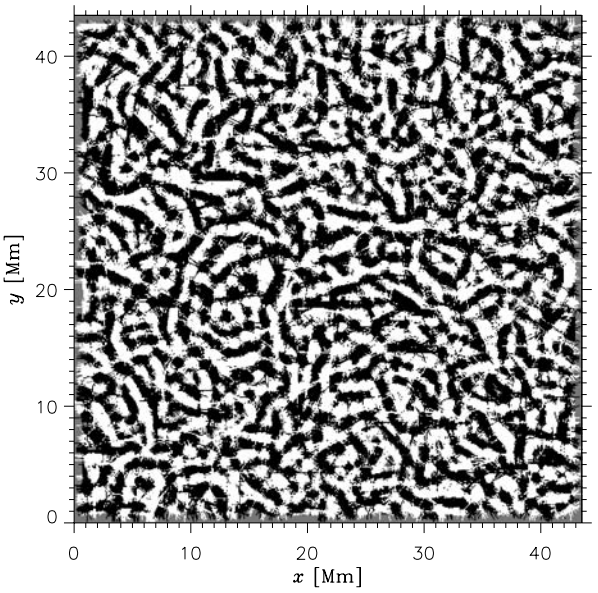

Figure 2 An illustration to the effect of the lineament-filtering procedure: the result of processing the image shown in Figure 1a at the same values of the processing parameters as in Figure 1c but without filtering.

As a rule, they are even less regular than the granular-scaled ridges; however, a system of very narrow parallel ridges can be distinguished near the upper left corner of the frame, within the (incomplete) white rectangle, as a pattern of very thin hatches inclined to the left. Thus, as we would expect, the characteristic scale of detectable features decreases with the decrease of Δ. However, if we reduce p by an order of magnitude (see panel b for example), too many features disappear, being treated by the code as "spurious." The remaining segments of curves are only the "most reliably identified" fragments of the structures, most parts of which have been filtered out. Nevertheless, even such drastically filtered patterns may be useful: the pattern enclosed in the (incomplete) white trapezoid in the upper left part of panel b suggests that a combination of concentric arcs and radial rays is present there, and it can be classified as a specific form of web pattern. [The occurrence of such patterns in averaged images was noted by Getling (2006)].

In the pattern of granular-scaled trenching, which is most pronounced in panel c, the structure marked by the white circle deserves particular attention. It appears as a system of concentric rings deformed and "spoiled" in some way and should therefore be included in our collection of ring systems. At the same time, it provides an example of a structure that can hardly be visually distinguished in the original image but which becomes detectable if the image is processed with a properly chosen parameter Δ $(= 8)$.

To illustrate the effect of the lineament-filtering procedure, we present here in Figure 2 the result of processing the image shown in Figure 1a at the parameters used to obtain Figure 1c but without filtering. It can easily be seen that the filtering procedure efficiently removes isolated bright blotches and very short lineaments, preserving more extended features and areas with pronounced trenching.

Figure 3 also refers to two-hour averaging. Here, panel a shows an averaged image for which the midtime of the averaging interval is nearly the same as for Figure 3 in Getling and Brandt (2002). This is still the best-available (most interesting) image, in terms of the presence of pronounced and highly ordered structures. The pattern in panel b was obtained by using the same parameters as in the case of Figure 1c. Encircled in the upper left quadrant is the well-developed system of concentric rings that appear as fairly regular circles

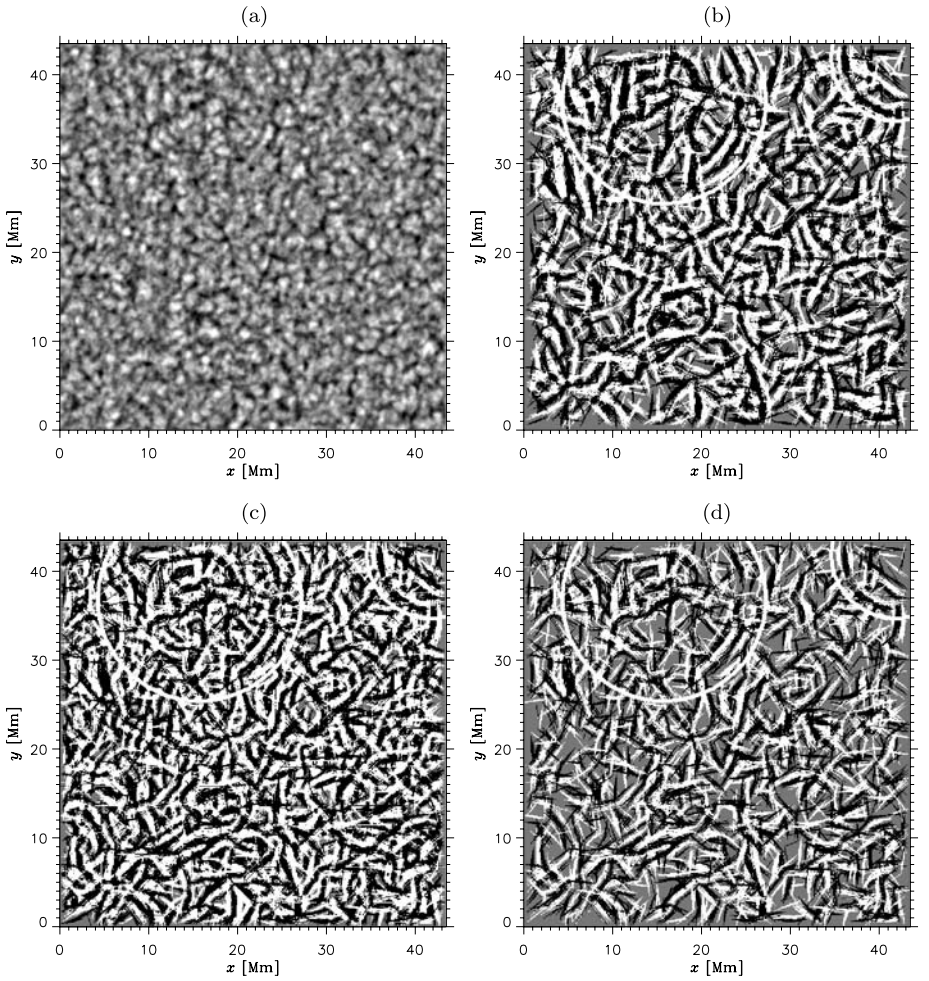

Figure 3 (a) Another two-hour-averaged image and the results of contour detection in it at (b) $p = 2 \times 10^{-3}$, $\Delta = 8$, $l = 10-30$; (c) $p = 10^{-2}$, $\Delta = 6$, $l = 10-20$; and (d) $p = 10^{-2}$, $\Delta = 6$, $l = 20$.

in panel a. Because of the presence of dark radial gaps interrupting the circles, the algorithm in some cases combines fragments of different rings into single contours, distorting the visual regularity of the system. A structure that may be part of another ring system, also marked with an (incomplete) circle, can be seen near the upper right corner of the frame. As in Figure 1c, even outside the regular structures, white lanes are accompanied by and alternate with black ones, and vice versa. In panel c, finer details are highlighted, since a smaller Δ is used in this case; in addition, p is here higher than for panel b. It is important that the main features present in the pattern do not disappear as p is reduced from 10^{-2} (c) to 2×10^{-3} (b), although the simultaneous increase of Δ additionally removes the narrowest lanes.

Finally, the effect of the l range can be understood by comparing panels c and d. The patterns shown in these panels were obtained at the same p and Δ but the range $l = 10-20$ was shrunk to the single value $l = 20$ with passing from panel c to panel d. Accordingly, short

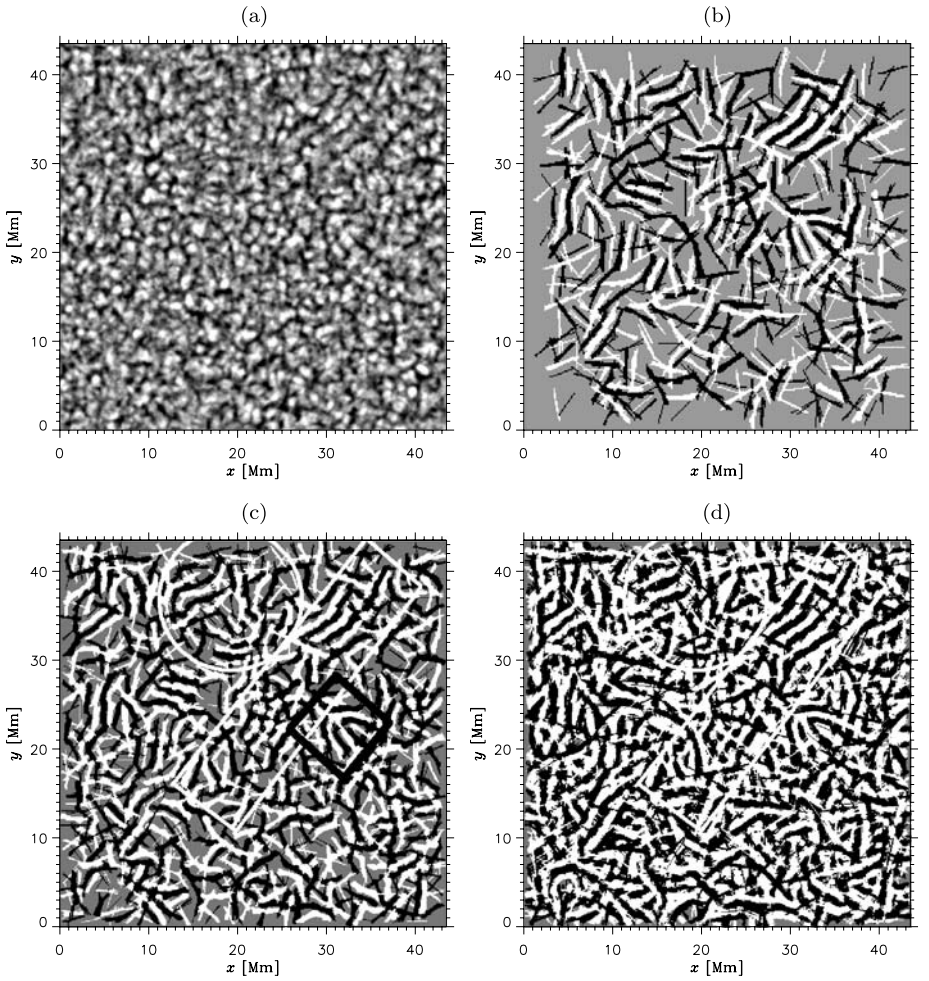

Figure 4 An image averaged over a one-hour interval centred at nearly the same time as in the case of Figure 1 and a comparison between the regimes of lineament and contour detection: (a) original image; (b) lineaments detected at $p = 10^{-3}$, $\Delta = 5$, $l = 16-43$; (c) lineaments detected at $p = 2.5 \times 10^{-4}$, $\Delta = 8$, $l = 16-43$; (d) contours detected at $p = 10^{-4}$, $\Delta = 8$, $l = 16-43$.

lineaments disappeared; however, objects exceeding 20 pixels in lengths were preserved because of combining partially overlapping lineaments into longer ones in the process of filtering and combining chains of lineaments into contours.

Thus, different combinations of parameter values can highlight different features in the image. To form a more complete idea of the structures present in the granulation field, the parameters at which the image is processed should be varied.

Whereas varying the image-processing parameters can be useful for the detection of features differing in their size, varying the averaging time makes it possible to reveal features differing in their lifetime. In this respect, it appears instructive to compare Figure 3, for

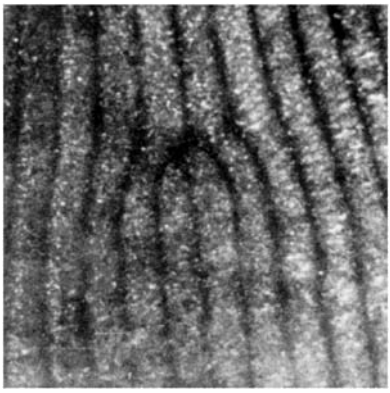

Figure 5 Dislocation in a roll-convection pattern (experimental photograph by Berdnikov and Markov).

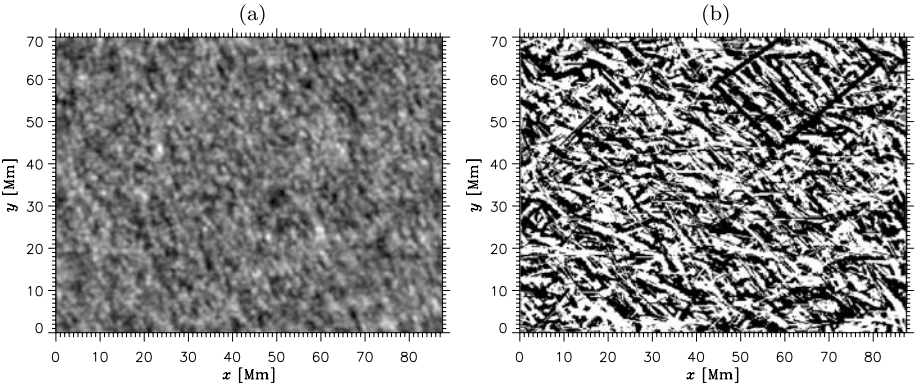

Figure 6 Processing of a two-hour-averaged MDI image: (a) original image; (b) the results of contour detection at $p = 5 \times 10^{-3}$, $\Delta = 2$, $l = 20$.

which the averaging time is two hours, with Figure 4, for which this time is one hour and the averaging interval is centred at virtually the same time as in the case of Figure 3.[1]

The original averaged image is given in Figure 4a; panels b and c present the results of processing it in a lineament-detection mode without filtering.[2] In both panels, there are many patches with a highly pronounced trenching. Panel c is considerably richer in ridge – trench systems than panel b, although the corresponding p value is one-quarter that for panel b. This is an additional illustration of the role of the parameter Δ. As in the examples just considered, the value $\Delta = 8$ is most favourable for the detection of contours of the fundamental width, and this fact proves here to be more important than some reduction of p.

It is interesting that the structure marked with a black box in Figure 4c is very similar to a fragment of a convection-roll pattern with a dislocation. Such patterns have received much attention in studies (particularly, experimental) of thermal convection (see, *e.g.*, Getling

[1] In Figure 4, where results obtained in both the lineament-detection and contour-detection modes are presented, they, by chance, appear very similar. In no way is this the general situation.

[2] The pattern shown in Figure 4b was obtained by using an older version of the code, which could not draw lineaments near the edges of the field of view.

(1998), for a survey); for comparison, we present an experimental photograph of a roll-convection pattern with a dislocation in Figure 5. (Obviously, this is merely an illustrative example; taken alone, it is insufficient to substantiate the claim that the observed feature is actually related to roll convection.)

The white rectangular box in Figures 4c and 4d (the latter panel representing the results of contour detection) marks an extended ridge – trench system, which is almost completely smeared in the two-hour-averaged image (Figure 3). The pattern within the white circle bears only faint resemblance to the pattern marked with the circle in Figures 3b – 3d, although some circular arcs can apparently be associated with the well-developed system present in Figure 3.

These observations clearly demonstrate that different features can be identified in the averaged images depending on the length of the averaging interval. In the case at hand, the system of concentric rings visible in Figure 3 appears to have a longer lifetime than has the elongated system identifiable in Figure 4.

Finally, we give here an example of processing results for an averaged image of the SOHO/MDI series (Figure 6). Panel a is an enlarged cutout of the subsonically filtered images of the MDI series averaged over a two-hour interval. As already noted by Getling (2006), this averaged image (also reproduced in that paper) exhibits a pattern of ridges and trenches in the form of overall "hatching" inclined to the right. The pixel size in the MDI series is about five times as large as in the La Palma series; accordingly, $\Delta = 2$ proves to be the optimum value for the detection of contours. The contour-detection results obtained at this value are shown in panel b. Generally, the $1.2''$ MDI resolution is insufficient for our algorithmic processing, and the code fails to detect the concentric-ring structures visible in panel a (and marked in Figure 1 in Getling (2006)). However, in some areas of the image, trenching patterns can be detected with certainty. A pattern of parallel ridges and trenches is highlighted most distinctly within the black box in the upper right quadrant of the field of view, where it appears highly ordered.

5. Conclusion

We have seen that the processing of time-averaged granulation images by the COLIBRI code is capable of detecting systems of ridges and trenches in the relief of the brightness field, which vary in their characteristic scale, geometry, and topology. The white lanes that highlight ridges are as a rule parallelled by one or more other white neighbouring lanes and at least two black lanes that mark trenches. Thus, our most general and remarkable finding is the fact that trenching patterns, irrespective of their particular geometries, are virtually ubiquitous in the averaged granulation images. The patterns may be more or less regular, and their patchy appearance is typical, but the property that they include alternating parallel white and black contours appears to be universal (provided the images analysed by us are representative).

The detection of objects differing in their sizes and other properties is possible if the parameters of image processing are properly chosen. Of particular importance is the adjustment of the parameter Δ to the characteristic width of ridges and trenches.

The patterns analysed here can most naturally be interpreted in terms of the structure of convective flows in the subphotospheric layers. If this interpretation is correct, the light ridges in the brightness field should correspond to material upflows, whereas the dark trenches can be associated with downflows. Accordingly, the parallelism of alternating ridges and trenches should be typical of roll convection, and, in the framework of our interpretation, roll motions seem to be virtually ubiquitous in the upper convection zone and

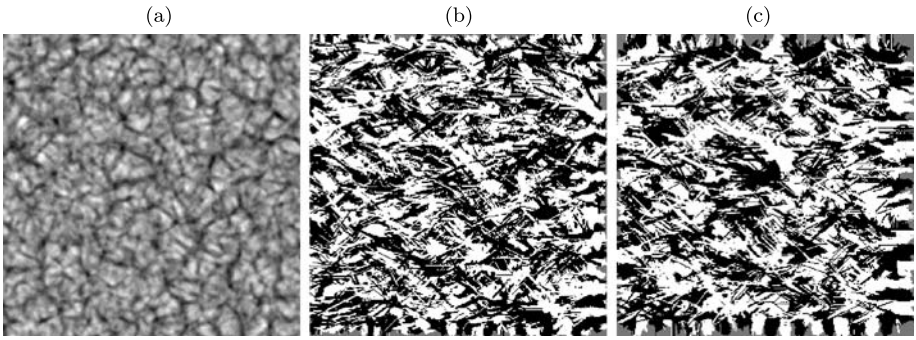

Figure 7 Processing of a simulated granulation field: (a) a two-hour average of the pattern obtained in simulations by Rieutord *et al.* (2002) and the results of contour detection in this averaged image with filtering at (b) $p = 0.01$, $\Delta = 8$, $l = 20$ and (c) at $p = 0.002 - 0.01$, $\Delta = 16$, $l = 20$.

photosphere of the Sun. However, under solar conditions, the hypothetical roll patterns are much more intricate in their structure than the roll patterns observed in laboratory experiments.

The outer diameters of the systems of concentric rings ("annular rolls") are of the order of the supergranular or mesogranular sizes, so such closed-ring systems could be an imprint of the fine structure of the supergranular or mesogranular flows in the subsurface layers.

The validity of our interpretation of the trenching patterns could be definitely stated only based on a comprehensive quantitative analysis. At the moment, the amount of information available is not yet sufficient for such an analysis and conclusion. Our aim here was merely to demonstrate, by representative examples, that the trenching patterns are widespread and diverse in their particular forms and that our algorithm can efficiently detect them. Nevertheless, we can now present here an illustration that appears to be an additional argument in favour of our interpretation.

We have averaged a series of images obtained in numerical simulations of granular-scaled solar convection by Rieutord *et al.* (2002). The computations covered a domain that corresponded to a 30×30 Mm^2 area of the solar photosphere. Each image contains 315×315 pixels of size 95.24 km, and the interval between images corresponds to 20 seconds of real time. A two-hour-averaged image is shown in Figure 7a; Figures 7b and 7c represent the results of processing the average using the COLIBRI code. It can easily be seen that, for widely ranging Δ (from 8 to 16 pixels), the code does not highlight any clear-cut ridges or trenches. The resulting image is not sensitive to variations in p over a range in which trenching was revealed in real solar images. It is thus fairly obvious that granular-sized polygonal convection cells cannot produce trenching patterns by themselves, and larger scaled convection must be responsible for the arrangement of granules that results in trenching.

The local brightness of a time-averaged image of the solar granulation reflects the local probability of the emergence of granules. The light blotches in the image indicate the sites where granules emerge most frequently. Qualitative reasoning (Getling, 2000) and correlation analyses (Getling, 2006) suggest that granules may be overheated blobs entrained by the convective circulation, and they can even repeatedly emerge on the solar surface. In this case, granules appear as markers of roll convective flows, which can thus be identified in averaged photospheric images.

Acknowledgements We are indebted to P.N. Brandt and R.A. Shine for making available the La Palma and SOHO MDI data, to T. Roudier for putting the results of numerical simulations at our disposal, and to

V.S. Berdnikov and V.A. Markov for providing the experimental photograph of a dislocation. We are also grateful to the referee and to L.M. Alekseeva for valuable comments on the manuscript. This work was supported by the Russian Foundation for Basic Research (Project Nos. 04-02-16580-a and 07-02-01094-a).

References

Baudin, F., Molowny-Horas, R., Koutchmy, S.: 1997, *Astron. Astrophys.* **326**, 842.
Berrilli, F., Del Moro, D., Consolini, G., Pietropaolo, E., Duvall, T.L. Jr., Kosovichev, A.G.: 2004, *Solar Phys.* **221**, 33.
Brandt, P.N., Getling, A.V.: 2004, In: Stepanov, A.V., Benevolenskaya, E.E., Kosovichev, A.G. (eds.) *Multi-Wavelength Investigations of Solar Activity*, *IAU Symp.* **223**, Cambridge University Press, Cambridge, 231.
Dialetis, D., Macris, C., Muller, R., Prokakis, T.: 1988, *Astron. Astrophys.* **204**, 275.
Getling, A.V.: 1998, *Rayleigh–Bénard Convection: Structures and Dynamics*, World Scientific, Singapore (Russian version: 1999, URSS, Moscow).
Getling, A.V.: 2000, *Astron. Zh.* **77**, 64 (English transl. *Astron. Rep.* **44**, 56).
Getling, A.V.: 2006, *Solar Phys.* **239**, 93.
Getling, A.V., Brandt, P.N.: 2002, *Astron. Astrophys.* **382**, L5.
Hoekzema, N.M., Brandt, P.N.: 2000, *Astron. Astrophys.* **353**, 389.
Hoekzema, N.M., Brandt, P.N., Rutten, R.J.: 1998, *Astron. Astrophys.* **333**, 322.
Lisle, J.P., Rast, M.P., Toomre, J.: 2004, *Astrophys. J.* **608**, 1167.
Mann, H.B., Whitney, D.R.: 1947, *Ann. Math. Stat.* **18**, 50.
Muller, R., Roudier, T., Vigneau, J.: 1990, *Solar Phys.* **126**, 53.
Rast, M.P.: 2002, *Astron. Astrophys.* **392**, L13.
Rieutord, M., Ludwig, H.-G., Roudier, T., Nordlund, Å., Stein, R.: 2002, *Nuovo Cimento* **25**, 523.
Roudier, T., Malherbe, J.M., November, L., Vigneau, J., Coupinot, G., Lafon, M., Muller, R.: 1997, *Astron. Astrophys.* **320**, 605.
Roudier, T., Lignières, F., Rieutord, M., Brandt, P.N., Malherbe, J.M.: 2003, *Astron. Astrophys.* **409**, 299.
Salov, G.I.: 1997, *Avtometriya*, No. 3, 60 (English transl. *Optoelectronics, Instrumentation and Data Processing*).
Shine, R.A., Simon, G.W., Hurlburt, N.E.: 2000, *Solar Phys.* **193**, 313.
Simon, G.W., Brandt, P.N., November, L.J., Scharmer, G.B., Shine, R.A.: 1994. In: Rutten, R.J., Schrijver, C.J. (eds.) *Solar Surface Magnetism*, *NATO Advanced Science Institute* **433**, Kluwer Academic, Dordrecht, 261.
Whitney, D.R.: 1951, *Ann. Math. Stat.* **22**, 274.